Available online at www.sciencedirect.com
ScienceDirect
Solid State Ionics 177 (2006) 3205–3210
SOLID STATE IONICS
www.elsevier.com/locate/ssi

Synthesis and investigations on the stability of $La_{0.8}Sr_{0.2}CuO_{2.4+\delta}$ at high temperatures

M. Zahid [a], I. Arul Raj [b], W. Fischer [a], F. Tietz [a,*], J.M. Serra Alfaro [a]

[a] *Forschungszentrum Jülich, Institute of Energy Research (IEF-1), D-52425 Jülich, Germany*
[b] *Central Electrochemical Research Institute, Karaikudi- 630006, India*

Received 11 May 2006; received in revised form 25 July 2006; accepted 31 July 2006

Abstract

For application in solid oxide fuel cells $La_{0.8}Sr_{0.2}CuO_{2.4+\delta}$ was synthesized and the phase evolution was characterized after quenching from different temperatures and after slow cooling. A single phase perovskite was found after quenching from 950 °C. The electrical conductivity of the $La_{0.8}Sr_{0.2}CuO_{2.4+\delta}$ perovskite exhibited metallic behavior reaching values of about 270 S/cm at 800 °C in air. The thermal expansion between 30 and 800 °C gave a thermal expansion coefficient of 11.1×10^{-6} K^{-1}.

At higher temperatures, the perovskite was transformed to the K_2NiF_4-type structure via an intermediate stage that can be best described as a $LaSrCuO_4$ phase with preferential growing of {020} lattice planes. After sintering at 1100 °C and slow cooling in the furnace a phase mixture of $(La,Sr)CuO_{4+\delta}$ and $(La,Sr)CuO_{2.4+\delta}$ perovskite was obtained. This phase mixture showed higher electrical conductivity (400 S/cm at 800 °C) and smaller thermal expansion coefficient (9.6×10^{-6} K^{-1}) than the single phase $La_{0.8}Sr_{0.2}CuO_{2.4+\delta}$ perovskite.

Keywords: Lanthanum cuprate; $La_{0.8}Sr_{0.2}CuO_{2.4+\delta}$; Phase transformation; Electrical conductivity; Thermal expansion

1. Introduction

Partially substituted binary and ternary perovskites from the series $La_{1-x}Sr_xMnO_{3-\delta}$ (LSM), $La_{1-x}Sr_xCoO_{3-\delta}$ (LSCo), $La_{1-x}Sr_xFeO_{3-\delta}$ (LSF), $La_{1-x}Sr_xNiO_{3-\delta}$ (LSN) and $La_{1-x}Sr_xCuO_{2.5-\delta}$ (LSCu) are widely investigated as they exhibit electronic or mixed conductivity as a function of composition, making them relevant for application either as catalysts [1], giant magneto-resistors [2], gas permeation membranes [3–5] and cathode or cathode/interconnect contact material in planar solid oxide fuel cells (SOFCs) [3,4,6–12]. Among these materials, $La_{1-x}Sr_xCuO_{2.5-\delta}$ has been studied for application as a high-temperature superconducting material [13,14] and also as an SOFC cathode [14]. Thermal and crystallographic stability of the $La_{1-x}Sr_xCuO_{2.5-\delta}$ perovskites is required for their application as a cathode/steel contact layer in planar SOFCs operating in the temperature range of 700–800 °C. They must also fulfil the requirements of high electrical conductivity and matching thermal expansion. It is reported that the stabilization of multivalent copper ions in the perovskite lattice is critical in order to obtain stable crystallographic and physical properties when considered for these applications [15,16]. However, during application in an SOFC no sophisticated treatments (e.g. heat treatment in pure O_2) can be tolerated and therefore the properties of $La_{1-x}Sr_xCuO_{2.5-\delta}$ have to be evaluated under ambient conditions.

Keeping this in mind, in the present work $La_{0.8}Sr_{0.2}CuO_{2.4+\delta}$ was investigated in more detail to obtain information on phase transformations occurring at different temperatures from a series of powder X-ray diffraction (XRD) analyses in order to define the processing conditions suitable for the stabilization of copper in the LSCu perovskite lattice. The A-site substitution with 20% Sr was selected, because this composition showed good compatibility with yttria-stabilized zirconia electrolytes [15] and it offers the possibility to compare the physical data with other $La_{0.8}Sr_{0.2}MO_{3-\delta}$ materials M=Mn,Co,Fe,Cu [4–10,12,15].

* Corresponding author.
E-mail address: f.tietz@fz-juelich.de (F. Tietz).

0167-2738/$ - see front matter © 2006 Elsevier B.V. All rights reserved.
doi:10.1016/j.ssi.2006.07.041

2. Experimental

2.1. Powder synthesis

The $La_{0.8}Sr_{0.2}CuO_{2.4+\delta}$ powder was synthesized by using the Pechini technique [17,18]. This involved weighing the appropriate quantity of the starting precursor salts $La(NO_3)_3 \cdot 6H_2O$, $Sr(NO_3)$, and $Cu(NO_3)_2 \cdot 3H_2O$ to obtain the targeted stoichiometry $La_{0.8}Sr_{0.2}CuO_{2.4+\delta}$ and dissolving them in de-ionized water. The resulting solution was mixed with citric acid in the molar ratio of 4 mol of citric acid to 1 mol of metal cations and stirred well at 40 °C. The resulting blue-colored solution was continuously stirred while being heated at 80 °C. After 3 h ethylene glycol was added stepwise. The volume of ethylene glycol added to the solution was a little more than the stoichiometric amount necessary to achieve complete polyesterification with the citric acid present in the solution. This mixture was heated at 220 °C and stirred continuously until most of the solvent had evaporated. The viscosity of the hot solution increased with time and stirring became difficult. The color of the solution turned to deep brown and then to black. During the preparation process, ignition was observed with the evolution of a deep brown stream of nitrogen oxides. The black mass obtained after complete evaporation was like resin and was dried in an oven in air at 230 °C for 6 h until it became coarse powder. This raw powder was ground well and subjected to calcination at 600 °C for 3 h in air.

2.2. Powder characterization

The powder obtained after calcination was analytically investigated by inductively coupled plasma atomic emission spectrometry (ICP-AES). The measured composition $La_{0.791}Sr_{0.199}Cu_{1.011}O_{2.4+\delta}$ was within the experimental accuracy of the method (±3 wt.%). The powder was also subjected to differential thermal analysis (DTA) combined with thermogravimetry (TG) in a Netzsch STA 409 to detect the melting point and the crystallization behavior.

2.3. Quenching experiments

In order to investigate the crystallographic features and to optimize the processing conditions of $La_{0.8}Sr_{0.2}CuO_{2.4+\delta}$ for application as electrically contacting material in an SOFC, the as-calcined powder was annealed in air at different temperature levels for 12 h each and quenched immediately in an ice bath for further characterization by powder XRD using a Siemens D5000 diffractometer with Cu K_α radiation. The annealing temperatures were fixed according to the DTA curve obtained with the as-calcined powder. Five different annealing experiments followed by immediate ice quenching were performed at 795, 859, 950, 1033 and 1086 °C.

2.4. Electrical conductivity and thermal expansion measurements

For DC electrical conductivity measurements rectangular bars (40 mm length, 4 mm width, 5 mm thickness) were fabricated by uniaxial pressing applying a pressure of 400 MPa for 120 s using glycerine as a pressing aid. The pressed rectangular bars were sintered in air at 950 °C for 6 h. The heating rate was 180 K/h.

The electrical conductivity of the sintered bars was measured by a standard four-point DC technique using a computerized set-up. Silver paste and wire were used to ensure good contacts on the specimens. The measurements were carried out in air between 50 and 900 °C. Considering the geometric uncertainties of the rectangular bars and the distances of the silver wires wrapped around them, the measured conductivity data have an experimental error of about ±4%.

The thermal expansion measurements were carried out with a Netzsch DIL 402 C dilatometer. The same sintered bars as for the conductivity measurements were used after cutting the length to 25 mm.

3. Results and discussion

3.1. DTA/TG Analysis

The DTA and TG curves obtained with the as-calcined powder are shown in Fig. 1a. The TG steps at 790 and 854 °C display the release of CO_2 due to the presence of carbonates in the raw

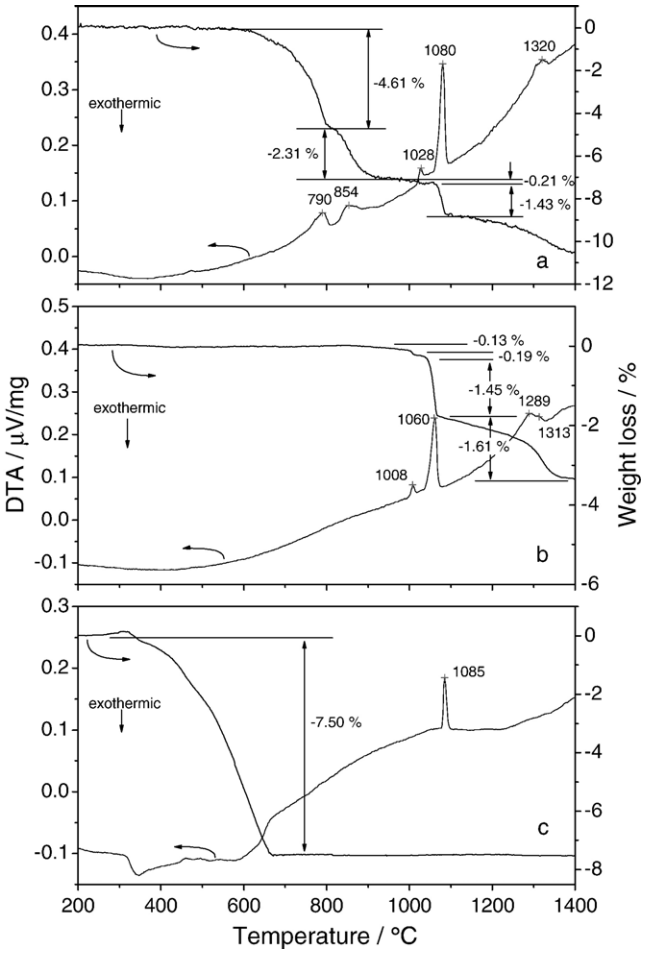

Fig. 1. DTA and TG curves of the $La_{0.8}Sr_{0.2}CuO_{2.4+\delta}$ powder after calcination at 600 °C for 3 h (a), after calcination at 950 °C for 6 h (b and c). The measurements (a) and (b) were performed in air, the measurement (c) was performed in Ar/4% H_2.

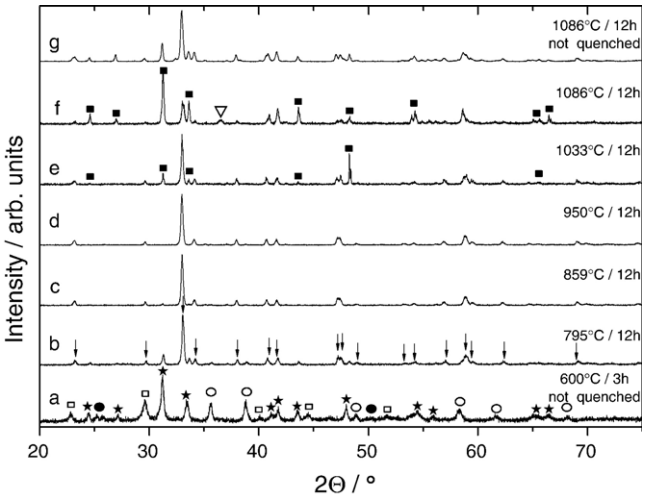

Fig. 2. XRD patterns of the powder after heat treatments at different temperatures: (a) 600 °C for 3 h and (g) 1086 °C for 12 h with subsequent natural cooling in the furnace, (b–f) annealing for 12 h at 795 °C (b), 859 °C (c), 950 °C (d), 1033 °C (e) and 1086 °C (f) and subsequent quenching. Symbols indicate the presence of $La_2O_2CO_3$ (open squares), $SrCO_3$ (solid circles), CuO (open circles), Cu_2O (open triangle), orthorhombic $La_2CuO_{4+\delta}$ (solid stars), tetragonal $LaSrCuO_{3.5+\delta}$ (K_2NiF_4-type, solid squares). The tetragonal perovskites are indicated by the arrows in (b).

powder after calcination at 600 °C. All the following steps can be related to transitions or reactions between the phases formed. Quenching experiments were performed to identify the crystal phases formed after the endothermal DTA signals and to determine the temperature at which the targeted perovskite structure crystallizes as a single phase. The annealing temperatures before quenching were chosen according to the endothermal DTA signals detected and the samples were heat-treated at 5 K above the peak temperatures as shown in Fig. 1a. The small peak at 1320 °C indicates the melting temperature of the sample.

After calcination at 950 °C for 6 h the single-phase powder was analyzed again in air and in Ar/4% H_2 to determine the oxygen content related to the mixed valency of copper. In air the DTA and TG curves show only signals at 1008, 1060 and 1289–1313 °C (Fig. 1b) corresponding to the signals at 1028, 1080 and 1320 °C after calcination at 600 °C. Although a temperature shift of about 20 °C is observed for the two differently crystallized powders, the weight losses at these temperatures are very similar.

In Ar/4% H_2, the weight loss is higher due to the reduction of the copper ions to metallic Cu.

The steps of phase transition and reduction can be expressed by the following reactions:

$$La_{0.8}Sr_{0.2}Cu^{II}_{1-x}Cu^{III}_{x}O_{2.4+x/2} \rightarrow La_{0.8}Sr_{0.2}Cu^{II}O_{2.4} + x/4\ O_2 \quad (1)$$

$$4\ La_{0.8}Sr_{0.2}Cu^{II}O_{2.4} \rightarrow 2\ La_{1.6}Sr_{0.4}Cu^{II}O_{3.8} + Cu_2O + 1/2\ O_2 \quad (2)$$

$$2\ La_{1.6}Sr_{0.4}Cu^{II}O_{3.8} + Cu_2O \rightarrow 1.6\ La_2O_3 + 0.8\ SrO + 4\ Cu + 1.7\ O_2 \quad (3)$$

Whereas the weight loss of Eq. (1) depends on the Cu^{3+} concentration, the other two weight losses related to the oxygen release in Eqs. (2) and (3) can be calculated to the theoretical values of 1.73% and 5.96%, respectively.

The initial oxygen content, i.e., the initial copper valence state, can be derived assuming that

(1) the weight losses are only related to the oxygen release during heating (Eqs. (1)–(3)),
(2) the small weight loss up to 1005–1030 °C is related to Eq. (1),
(3) the sharp weight loss around 1060–1080 °C is related to Eq. (2),
(4) the following slow weight loss up to 1290 °C in air is related to a continuous phase decomposition of the K_2NiF_4 phase and increasing content of Cu_2O. The formation of Cu_2O is confirmed by XRD measurements (see Fig. 2).

The weight losses during different measurements are summarized in Table 1. The total weight loss from Eqs. (2)

Table 1
Weight losses during DTA/TG measurements and associated reactions (see also text)

Powder history	Atmosphere during measurement	Temperature range (°C)	Weight loss (%)	Process
Powder after calcination at 600 °C for 3 h	air	550–810	4.61	Decomposition of lanthanum and strontium carbonate
		810–970	2.31	
		970–1050	0.21	Eq. (1)
		1050–1110	1.43	Eq. (2)
		1110–1320	1.07	Decomposition before melting
Powder after calcination at 600 °C for 3 h and 950 °C for 6 h	air	850–1004	0.13	Eq. (1)
		1004–1036	0.19	Eq. (1)
		1036–1066	1.45	Eq. (2)
		1066–1290	0.78	Decomposition before melting
		1290–1400	0.82	Decomposition after melting
Powder after calcination at 600 °C for 3 h and 950 °C for 6 h	Ar	675–965	0.41	Eq. (1)
		965–990	0.20	Eq. (1)
		990–1043	1.63	Eq. (2)
		1043–1300	1.65	Decomposition before melting
Powder after calcination at 600 °C for 3 h and 950 °C for 6 h	Ar/4% H_2	300–640	7.5	Eqs. (1)–(3)

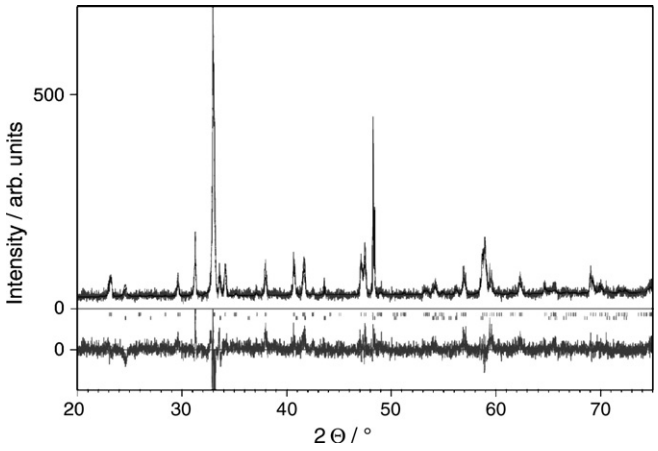

Fig. 3. Rietveld plot of the powder pattern after annealing at 1033 °C and subsequent quenching. Upper window: measured pattern dark gray, fitted curve black, lower window: differential plot dark gray, upper markers indicate LSCu reflections, lower markers $LaSrCuO_4$ reflections.

and (3) of about 7.7% is confirmed by a DTA/TG measurement in Ar/4% H_2 (Fig. 1c). The peak at 1085 °C is the melting point of metallic Cu. The theoretical weight loss of 1.73% of Eq. (2) is not reached during the measurements in air. The measured values of 1.44±0.01% (Fig. 1a and b) indicate that this reaction is either not completed or the formed $(La,Sr)CuO_{4-\delta}$ contains mixed-valent Cu ions.

Taking into account the molar weight of $La_{0.8}Sr_{0.2}Cu^{(II)}O_{2.4}$, the weight difference between 850 and 1036 °C (0.32% for the measurement in air, Table 1) gives an amount of oxygen of 0.045 mol/formula unit (f.u.). This leads to a sample stoichiometry of $La_{0.8}Sr_{0.2}CuO_{2.445}$ and a copper valence state of $Cu^{2.09}$ under ambient conditions. The fraction of Cu^{3+} ions of 9% is lower than 14.2% obtained in [15], probably due to the different experimental conditions.

3.2. XRD data

The XRD results of the heat treated samples are presented in Fig. 2. No perovskite was formed after calcination at 600 °C for 3 h (Fig. 2a). Due to the low calcination temperature, carbonates like $La_2O_2CO_3$ (open squares) and $SrCO_3$ (closed circles) as well as tenorite (CuO, open circles) can be detected. The major crystal phase detected after calcination was the orthorhombic La_2CuO_4-like compound (space group Fmmm, JCPDS file no. 30-0487, solid stars).

From this calcination temperature upwards, the evolution of the crystal phases proceeds through several stages. (i) In the range between 600 °C and 859 °C a gradual decrease in intensity of the reflections of the $La_2CuO_{4+\delta}$-like compound (L2Cu) was observed. This trend was accompanied by the crystallization of the tetragonal perovskites (LSCu) with an XRD pattern similar to $La_{0.75}Sr_{0.25}CuO_{2.44}$ (JCPDS file no. 46-0653, indicated by the arrows in Fig. 2b) and by the disappearance of all carbonate phases. After annealing at 859 °C for 12 h small amounts of L2Cu and CuO can be detected as impurities and LSCu became the main phase. (ii) At 950 °C only the tetragonal perovskite $La_{0.8}Sr_{0.2}CuO_{2.4+\delta}$ was detected as a single phase. (iii) At 1033 °C the formation of the tetragonal $LaSrCuO_4$ compound (space group I4/mmm, JCPDS file no. 27-1132, solid squares) with K_2NiF_4-type crystal structure was observed. This was accompanied by the decrease in intensity of the reflections of the $La_{0.8}Sr_{0.2}CuO_{2.4+\delta}$ tetragonal perovskite phase indicating a phase transition of the perovskite to the K_2NiF_4-type crystal structure. However, the XRD pattern for the quenched sample after annealing at 1033 °C for 12 h shows a sharp peak at 2Θ=48.29° with very high intensity indicating a preferred orientation of the phase transition from the tetragonal perovskite to the K_2NiF_4-type crystal structure. At 1086 °C cuprite (Cu_2O, open triangle) was detected as an impurity.

Rietveld refinement [19] was applied to elucidate the atomistic processes taking place during the phase transformation from tetragonal perovskite to tetragonal K_2NiF_4-type structure at about 1033 °C. The single-phase XRD pattern of the powder recorded after annealing at 950 °C was used to calculate the unit cell of LSCu. Starting with the crystal structure of tetragonal $La_{4.4}Sr_{3.6}Cu_6Fe_2O_{20}$ (ICSD collection code no. 79454) [20] and introducing site substitutions according to the actual composition, the unit cell was refined with respect to its metric. This adopted structure of LSCu allowed an easier splitting of the powder pattern at 1033 °C, which is a superposition of the two tetragonal sub-patterns. The reflections of the second phase are best matched by $LaSrCuO_4$ (PDF 27-1132). The unit cell of this phase (ICSD collection code no. 10525) has been described in [21]. A satisfactory fit of the sub-pattern of this second phase was achieved by only assuming pronounced preferential orientation. Several orientations were checked with the result that an (020) texture gave the best fit to the measured pattern. Fig. 3 shows a comparison of the measured and the fitted patterns as well as the difference plot. There is a good agreement within the limits of the quality of the measured pattern, keeping in mind that only the metric of the unit cell has been refined. This result indicates that the phase transformation proceeds either via a preferential

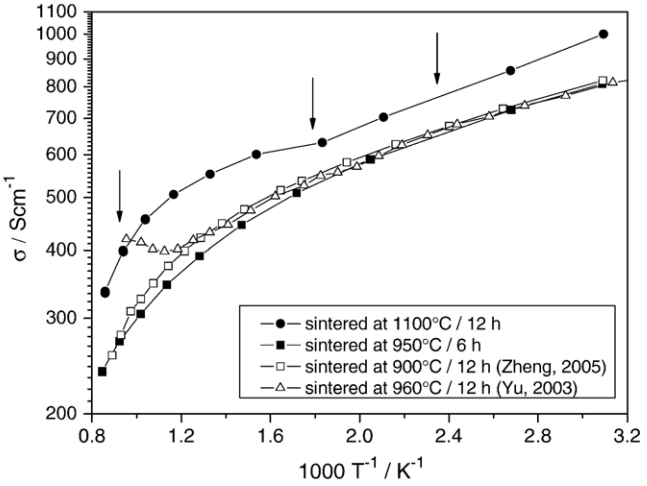

Fig. 4. Electrical conductivity as function of temperature and sintering conditions: (●) after sintering at 1100 °C for 12 h, (■) after sintering at 950 °C for 12 h, (□) after sintering at 900 °C for 12 h, data taken from [22] and (△) after sintering at 960 °C for 12 h, data taken from [23]. The arrows indicate the quenching temperatures T_q=150, 400 and 800 °C to identify reasons for the slope changes in the conductivity curve.

growing of {020} lattice planes, which might represent the nuclei for further phase formation, or with the formation of an intermediate and metastable phase with a pronounced texture.

3.3. Electrical conductivity and thermal expansion

The specific electrical conductivity values after correction for porosity [12] of a sample sintered at 950 °C for 6 h in air (34% of porosity) is shown in Fig. 4. These values are in good agreement with measurements reported in [22], whereas the data reported in [23] deviate from 550 to 800 °C. The sample, being single phase according to Fig. 2, exhibited a metal-like behavior according to the decrease of conductivity with increasing temperature reaching values of about 270 and 350 S/cm at 800 and 600 °C in air, respectively. The same behavior can be observed for the sample sintered at 1100 °C for 12 h and cooled down at 3 K/min in air. However, the measured electrical conductivity is significantly higher reaching values of about 400 S/cm at 800 °C in air. Also here the 14.6% of porosity of the sample was taken into account for the calculation of the specific electrical conductivity. However, besides the porosity also the better grain connectivity leads to an increase in conductivity. The slope changes of the curve, however, can be attributed to the change of phase content in the sample (Fig. 2g, see also further below). While in the sample sintered at 950 °C the LSCu perovskite appears as a single phase, the sample sintered at 1100 °C contains mainly a compound with K_2NiF_4-type structure and LSCu as a secondary phase.

The thermal expansion of the sample sintered at 950 °C for 6 h in air was determined at temperatures between 30 and 1000 °C in air and is presented in Fig. 5 as curve *a*. Up to 950 °C the sample shows a nearly constant slope and the thermal expansion coefficient (TEC) between room temperature and 800 °C is 11.1×10^{-6} K^{-1}. This value is strongly deviating from the formerly reported TEC of 17.9×10^{-6} K^{-1} [15]. At 950 °C the slope is strongly increased up to 1000 °C indicating a change within the sample that can be explained according to Fig. 1 by the release of oxygen from the perovskite lattice. It is interesting to note that during a subsequent

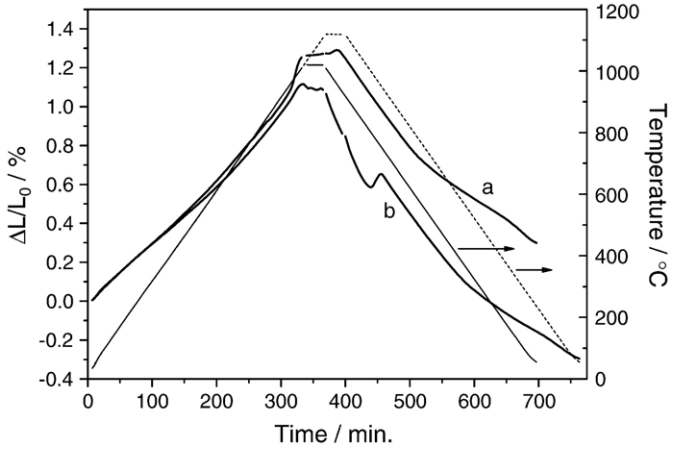

Fig. 5. Thermal expansion curves during heating and cooling at 3 K/min of $La_{0.8}Sr_{0.2}CuO_3$ after sintering at 950 °C. The first measurement was carried out up to 1000 °C (solid line), the second measurement was extended to 1100 °C (dashed line). After heating up, in both cases a dwell time of 0.5 h followed at maximum temperature before the samples were cooled down again.

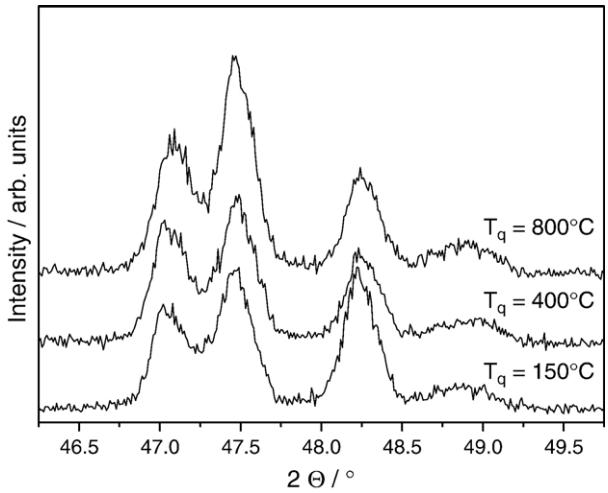

Fig. 6. Enlarged part of the XRD patterns of samples sintered at 1100 °C for 12 h, slowly cooled to the quenching temperature (T_q) and subsequently quenched from this temperature (see also arrows in Fig. 4).

isothermal dwell time the lattice does not expand further whereas during cooling this process seems to continue and the sample further expands at high temperatures instead of showing a hysteresis. A more detailed investigation is necessary to understand this anomaly. In a second measurement (curve *b* in Fig. 5) the sample was heated up to 1100 °C in a similar manner to the heat treatment for the electrical conductivity measurements. An increase of the slope starting at 950 °C was also observed here. However, at temperatures higher than 1000 °C the phase transformation competes with a further densification and sintering of the sample leading to a shrinkage of the sample during isothermal dwell time. During cooling a phase transition is observed between 950 and 1000 °C, and in addition both cooling curves show a small change of the slope at about 500 °C that coincides with the slope change during the conductivity measurements (Fig. 4). The TEC between room temperature and 800 °C, determined from the cooling curves, is 10.2 and 9.6×10^{-6} K^{-1} after heating the sample to 1000 and 1100 °C, respectively.

To understand these slope changes, after the same heat treatments as for the conductivity measurements, three samples were additionally quenched from 800, 400 and 150 °C as indicated by the arrows in Fig. 4. The XRD patterns indicate a continuous variation of the crystallographic phases (Fig. 6). Between 800 and 400 °C the relative intensity of the reflection at 47.5° ((440) reflection of the tetragonal perovskite $La_{0.8}Sr_{0.2}CuO_{2.4+\delta}$) is significantly reduced, whereas between 400 and 150 °C the peak at 48.2 ((200) of the tetragonal $LaSrCuO_{3.5+\delta}$) increased. Small changes in the phase composition seem to be the reason for the slope changes of the electrical conductivity curve (Fig. 4).

4. Conclusion

Information on the evolution of crystallographic stability in $La_{1-x}Sr_xCuO_{2.4+\delta}$ perovskites was collected in order to determine the applicability of these materials for SOFCs. Investigating the temperature-dependent phase transformations from a series of

powder XRD experiments after selected annealing conditions, it was found that $La_{0.8}Sr_{0.2}CuO_{2.4+\delta}$ can be obtained as a single-phase tetragonal perovskite after annealing at 950 °C for 12 h in air. This perovskite undergoes a continuous crystallographic transformation to the K_2NiF_4 structure after annealing above 1033 °C via a highly oriented intermediate structure growing along {020} lattice planes. DC electrical conductivity measurements for this composition indicated a metallic behavior reaching values of about 270 to 400 S/cm at 800 °C in air depending on the annealing temperature and hence on the phase content in the specimens, whereas the TEC from 30 °C to 800 °C varied between 11.1 and 9.6×10^{-6} K^{-1}, respectively.

The presented investigations on $La_{0.8}Sr_{0.2}CuO_{2.4+\delta}$ show that this compound is an attractive candidate for SOFC application as long as the assembling and stack operation does not exceed a temperature of 950 °C. In such cases, the perovskite is partially transformed into a K_2NiF_4-type phase that shows a higher electrical conductivity but also a small TEC, which is less attractive with respect to thermal cycling.

Acknowledgements

J. M. S. is indebted to Fundación Ramón Areces for institutional and financial support. The authors thank the Central Department of Chemistry of FZJ for the chemical analysis of samples.

References

[1] M.A. Peña, J.L.G. Fierro, Chem. Rev. 101 (2001) 1981.
[2] N. Zhang, W. Ding, W. Zhong, D. Xing, Y. Du, Phys. Rev., B 56 (1997) 8138.
[3] H.J.M. Bouwmeester, Catal. Today 82 (2003) 141.
[4] A. Petric, P. Huang, F. Tietz, Solid State Ionics 135 (2000) 719.
[5] V.V. Kharton, A.A. Yaremchenko, A.L. Shaula, A.P. Viskup, P.M.B. Marques, J.R. Frade, E.N. Naumovich, J.R. Casanova, I.P. Marozau, Diffus. Defect Data Solid State Data, Pt. A Defect Diffus. Forum 226–228 (2004) 141.
[6] L.-W. Tai, M.M. Nasrallah, H.U. Anderson, D.M. Sparlin, S.R. Sehlin, Solid State Ionics 76 (1995) 259.
[7] E. Ivers-Tiffée, A. Weber, D. Herbstritt, J. Eur. Ceram. Soc. 21 (2001) 1805.
[8] R. Chiba, F. Yoshimura, Y. Sakurai, Solid State Ionics 124 (1999) 281.
[9] F. Riza, C. Ftikos, F. Tietz, W. Fischer, J. Eur. Ceram. Soc. 21 (2001) 1769.
[10] P. Gordes, N. Christiansen, F.W. Poulsen, L. Bouakaz, K. Thomsen, in: F.W. Poulsen, N. Bonanos, S. Linderoth, M. Mogensen, B. Zachau-Christiansen (Eds.), Proc. 17th Risø Int. Symp. Materials Science, Risø National Laboratory, Roskilde, 1996, p. 247.
[11] G.C. Kostogloudis, C. Ftikos, Solid State Ionics 126 (1999) 143.
[12] M. Zahid, I. Arul Raj, F. Tietz, P. Lersch, D. Stöver, in: S.C. Singhal, J. Mizusaki (Eds.), Proc. 9th Int. Symp. Solid Oxide Fuel Cells (SOFC-IX), vol. 2, The Electrochemical Society, Pennington, NJ, 2005, p. 1708.
[13] Y. Khan, J. Mater. Sci. Lett. 6 (1987) 387.
[14] C. Michel, L. Er-Rakho, B. Raveau, Mater. Res. Bull. 20 (1985) 667.
[15] H.-C. Yu, K.-Z. Fung, J. Power Sources 133 (2004) 162.
[16] S. Darracq, S.G. Kang, J.H. Choy, G. Demazeau, J. Solid State Chem. 114 (1995) 88.
[17] M.P. Pechini, US Patent No. 3,330,697, (1967).
[18] F. Tietz, I. Arul Raj, W. Jungen, D. Stöver, Acta Mater. 49 (2001) 803.
[19] R.A. Young, The Rietveld Method, International Union of Crystallography, Oxford University Press, 1993.
[20] R. Genouel, C. Michel, N. Nguyen, M. Hervieu, B. Raveau, J. Solid State Chem. 115 (1995) 469.
[21] J.B. Goodenough, G. Demazeau, M. Pouchard, P. Hagenmüller, J. Solid State Chem. 8 (1973) 325.
[22] M. Zheng, X. Liu, W. Su, J. Alloys Compd. 395 (2005) 300.
[23] H.-C. Yu, K.-Z. Fung, Mater. Res. Bull. 38 (2003) 231.